JOURNAL OF CATALYSIS 100, 118–129 (1986)

Spectroscopic and Catalytic Study on Metal Carbonyl Clusters Supported on Cab-O-Sil

III. Application of Low-Temperature, High-Field Mössbauer Spectroscopy and Ferromagnetic Resonance for Characterizing FeRu Bimetallic Catalysts

K. LÁZÁR,* W. M. REIFF,†,[1] W. MÖRKE,‡ AND L. GUCZI*,[1]

*Institute of Isotopes of the Hungarian Academy of Sciences, P.O. Box 77, H-1525 Budapest, Hungary; †Department of Chemistry, Northeastern University, Boston, Massachusetts 02115; and ‡Department of Chemistry, Technical University "Carl Schorlemmer," 4200 Merseburg, Germany (DDR)

Received September 27, 1984; revised October 8, 1985

Low-temperature, high external magnetic field Mössbauer spectroscopy and ferromagnetic resnance were used to characterize iron and iron–ruthenium bimetallic catalysts derived from molecular clusters and supported on Cab-O-Sil. The Ru/Fe ratio varied between 1.6 and 6.0. These two methods enabled it to be unambiguously established that paramagnetic iron–ruthenium bimetallic particles of high dispersion are always present along with iron oxide after reduction at high temperature and in the CO + H_2 reaction. Thus, for the catalysts investigated earlier (see *J. Catal.* **87,** 179, 1984) the catalytic behavior is attributable to iron–ruthenium bimetallic particles. A value of 3 nm has been estimated for the diameter of ferromagnetic metallic particles.

INTRODUCTION

Iron and ruthenium exhibit catalytic activity in the CO + H_2 reaction, but for iron there is a decay in the catalytic activity due to the formation of inactive carbides. Alloying iron with ruthenium results in a significant improvement in the stability of the catalytic system compared with a one-component iron catalyst (*1, 2*).

Supported iron–ruthenium catalysts are assumed to combine the benefits of high dispersion and alloying. The existence of an iron–ruthenium interaction has been revealed mainly by determining the product distribution in the CO + H_2 reaction and studying the oxidation–reduction cycles of these supported catalysts. Using Mössbauer spectroscopy, Vannice *et al.* (*3*) found that ruthenium enhances the room-temperature reducibility of Fe^{3+} to Fe^{2+} at high Ru/Fe ratios on silica-supported catalysts with high metal loading. The doublet with an isomer shift of 0.38 mm s^{-1} and quadrupole splitting of 0.73 mm s^{-1} was assigned by these authors to a surface iron–ruthenium bimetallic cluster. Niemantsverdriet *et al.* (*4*) recently disagreed with this assignment in view of their experimental results on CO and NH_3 chemisorption in which this doublet was assigned to Fe^{3+} species. Here the single line at 0.0 mm s^{-1} in the room-temperature Mössbauer spectra was attributed to Fe–Ru alloy particles.

At low metal loading (at or below 1 wt% metal) no sign of $Fe^{(0)}$ was observed (*5*) and even the reduction of Fe^{3+} to Fe^{2+} was difficult on zeolites in the presence of ruthenium.

However, using a mixture of $Fe_3(CO)_{12}$ and $Ru_3(CO)_{12}$ on Cab-O-Sil the resulting catalytic activity (per unit weight of metal) in the CO + H_2 reaction appeared to be at least one order of magnitude higher than any other bimetallic catalysts prepared from inorganic salt solution by the incipient wetness method (*6*). In addition, the observed selectivity is also indicative of the formation of bimetallic catalysts. Regardless of the source of the molecular cluster

[1] To whom correspondence should be addressed.

0021-9517/86 $3.00

(i.e., whether it is a mixture of two monometallic clusters or a bimetallic cluster) the same behavior was found (*7–12*).

Infrared spectroscopy has provided evidence that interaction between $Fe_3(CO)_{12}$ and $Ru_3(CO)_{12}$ commences during decomposition (*9*). On the other hand, if the starting material is a molecular bimetallic cluster, disintegration of the cluster framework occurs at 370 K with the formation of iron oxide and ruthenium carbonyl species (*13*). Similar behavior has been observed for other bimetallic systems such as $H_2FeOs_3(CO)_{13}$ (*14*) and $H_2RuOs_3(CO)_{13}$ (*15*). Carbon-supported iron–ruthenium catalysts prepared from bimetallic clusters and from a mixture of iron plus ruthenium carbonyls displayed distinct differences in their catalytic behavior, the latter catalyst being less homogeneous than the former (*16*). However, regardless of the carbonyl cluster source, after high-temperature reduction in hydrogen the catalytic activity and selectivity displayed in the $CO + H_2$ reaction reveal the existence of bimetallic species. In addition, other data also point to the presence of bimetallic particles, e.g., carbide formation—which is a common feature on iron—is retarded in the presence of ruthenium (*10*). However, this phenomenon might be ascribed to the presence of very small particles, as was assumed by Blanchard *et al.* (*17*). For aerogel-supported Fe_2O_3, these authors reported that the formation of α-iron is hindered, carbide phase formation is suppressed, and high catalytic activity is maintained.

Since there is no direct evidence to support the presence of iron–ruthenium bimetallic particles, high-field Mössbauer spectroscopy may be useful for studying the iron–ruthenium catalysts. This method represents a tool for distinguishing between different magnetic behaviors of the metallic species formed in the catalysts during high-temperature treatments. The method has been successfully applied to investigate a silica-supported 5 wt% Fe + 5.3 wt% Co catalyst; the formation of Fe–Co bimetallic particles has been detected after different treatments (*18*).

Other magnetic studies can also provide valuable information on supported catalysts. The presence of the ferromagnetic iron particles was revealed from static magnetic measurements performed on carbon-supported iron catalysts (*19*). Ferromagnetic resonance (FMR) spectroscopy is also an efficient method for studying supported catalysts. The shape and the intensity of the signal are closely correlated with the form (*20*), structure (*21*), and the size distribution (*22*) of ferromagnetic particles. Information on the first two parameters can be obtained from the simulation of FMR spectra (*23*); the size distribution can be determined from the temperature dependence of the intensity of the measured signal (*24*). Alloy formation can also be revealed from the measurements as has been reported, for example, on Cu–Ni particles on a silica support (*25*). Decomposition products of iron carbonyls supported on magnesia (*26*) and silica (*27*) were also studied by FMR and in both cases metallic iron was found as the main product.

In the present work we are concerned mainly with the characterization of metallic particles in the Fe–Ru system, and in particular with the formation or iron–ruthenium bimetallic particles after reduction and under catalytic conditions. For this purpose a mixture of $Fe_3(CO)_{12}$ and $Ru_3(CO)_{12}$ as well as $H_2FeRu_3(CO)_{13} + H_2Fe_2Ru_2(CO)_{13}$ supported on Cab-O-Sil have been used with a Ru/Fe ratio between 1.6 and 6. Low-temperature (~1.5 K) Mössbauer spectra complemented by external magnetic fields up to 8 T as well as ferromagnetic resonance allow us to obtain detailed structural information for these samples.

EXPERIMENTAL

Sample preparation. All samples were deposited on a Cab-O-Sil HS5 support (Cabot Corp., Tuscola, Ill.). Prior to the impregnation, the support was evacuated

overnight at 570 K. The apparatus used and further details of the impregnation are described in Part I (*8*). Samples 1 and 2 were made by a two-step impregnation process. First, the support was impregnated with iron dodecacarbonyl solution, then after 4 h of room-temperature drying under vacuum, ruthenium dodecacarbonyl was added from the second solution prepared from ethanol or dimethyl ether. Iron dodecacarbonyl was synthesized from iron isotopically enriched with 50% ^{57}Fe. Due to the difficulties in the microsynthesis of the bimetallic molecular cluster containing ^{57}Fe, separation of $H_2Fe_2Ru_2(CO)_{13}$ and $H_2FeRu_3(CO)_{13}$ could not be carried out without significant loss of ^{57}Fe; thus, a mixture of the two molecules in a 3 : 1 ratio was used for impregnation. The total metal loading was 1–2 wt% where the metal percentage was determined by X-ray fluorescence. The hydrogen employed in decomposition and reduction was purified using a supported Pd catalyst followed by a cold trap at liquid-nitrogen temperature. The carbon monoxide (99.95% pure) used for the high-temperature CO + H_2 reaction was supplied by Linde Company.

Apparatus and procedure. The low-temperature measurements were carried out in "Super-Vari-Temp" flow-gas cryostats (Janis Res. Co.); the cryogen gas flushed the sample. The measurements below 4.2 K were performed at reduced He pressure in the sample chamber. The temperature measurement and control were based on calibrated and uncalibrated silicon diodes, respectively.

The high-temperature treatments were carried out in a furnace made for *in situ* Mössbauer measurements (Janis Res. Co.); the apparatus was similar to that described previously (*8*), but without the possibility of cooling the sample holder inside the furnace. The CO + H_2 reaction mixture and the hydrogen flowed directly over the sample. A chromel–alumel thermocouple was used to measure and control the temperature (±1 K).

The external magnetic field for the Mössbauer measurements was generated by a liquid-helium-cooled niobium–titanium superconducting magnet with the applied field being parallel to the γ-ray propagation direction. The maximum value of the field strength was 8 T at 4.2 K. The Mössbauer spectrometer drive-rod/sample-holder assembly was incorporated with the foregoing superconducting magnet cryostat in the vertical mode with the γ-ray source and absorber at the same temperature.

A 40-mCi ^{57}Co (diffused into a rhodium matrix) γ-ray source was used at ambient temperature, except for the high-field measurements. Metallic iron foil was used for the velocity calibrations and all of the isomer shift values are related to α-iron. The accuracy of the reported isomer shifts (IS) and magnetic splitting (H_{eff}) values are ±0.02 mm s^{-1}) and ±1.5 kOe, respectively.

Mössbauer spectra were collected in Canberra 35, Elscint Promeda and Tracor Northern TN-1706 multichannel analyzers. The programs BURNS and SIRIUS were used for fitting the spectra. The procedure of the calculation assumes a Lorentzian shape for the Mössbauer lines (*28*). Usually only the number of lines was constrained in the fits of spectra (the exceptions are indicated in the text).

FMR spectra were recorded on an X-band (9.3 GHz) spectrometer (ERS 220 type) with 100 kHz modulation at various temperatures. A copper–constantan thermocouple was used to control the temperature (±1 K). Two parameters of the FMR spectra were used to characterize the signals, viz. the intensity I, and the linewidth ΔH_{pp} (I was calculated using the equation $I = I' \Delta H_{pp}^2$, where I' is the peak-to-peak height and ΔH_{pp} is the width measured between the two extreme values of the signal). A further parameter, the relative intensity I_r, was also used to characterize the samples. This parameter is defined as the intensity ratio of the signal obtained at a given temperature related to that measured at the lowest temperature ($0 < I_r \leq 1$).

TABLE 1

Composition and Treatment of Samples[a]

Sample	Starting material	Ru/Fe ratio	Treatment/T(K)
1	$Fe_3(CO)_{12}$ hexane $Ru_3(CO)_{12}$ ethanol	3.9	$CO + H_2$ 570
2	$Fe_3(CO)_{12}$ hexane $Ru_3(CO)_{12}$ ether	6.5	Hydrogen 650
3	$H_2Fe_2Ru_3(CO)_{13}$ and $H_2FeRu_3(CO)_{13}$ hexane	1.6	$CO + H_2$ 610
4	$Fe_3(CO)_{12}$ hexane	0	$CO + H_2$ 650

[a] Before treatment all samples were decomposed in hydrogen at 370 K.

For sample characterization, the supported carbonyl was first decomposed in hydrogen at 370 K for 3 h. The sample was then either reduced in hydrogen at 650 K or treated by a $CO + H_2$ reaction mixture for a period between 2 and 7 days. After cooling in hydrogen or in the $CO + H_2$ mixture the sample was covered and sealed in a heat-resisting plastic (Vespel) sample holder. Prior to sealing the sample, the furnace used for the high-temperature treatments had to be dismantled. Although this procedure was carried out under an argon atmosphere, a trace amount of oxygen might have diffused to the sample. Diffusion of oxygen would affect only valence state of the oxide component.

After being sealed the sample was transferred into the cryostat for the low-temperature Mössbauer characterization. Details on the composition and treatment of the samples are presented in Table 1.

FMR measurements were performed on the samples after their Mössbauer characterization. First, all samples were reduced in hydrogen at 650 K for 1 h. They were then cooled and sealed in FMR test tubes in an argon atmosphere.

RESULTS

Impregnation of Cab-O-Sil either by a hexane solution of a bimetallic iron–ruthenium carbonyl cluster (*29*) or by the dissolved mixture of the two monometallic carbonyl clusters (*13*) has revealed two different types of behavior. In the former case the impregnated form of the bimetallic cluster appeared to be stable whereas for the mixture iron oxide was always formed after impregnation as a result of the interaction of surface hydroxyl groups and zerovalent iron. Similar behavior was observed after decomposition in hydrogen at 370–400 K. However, after high-temperature reduction, besides the doublets of high-spin Fe^{2+} and Fe^{3+} oxides some $Fe^{(0)}$ was observed in the form of superparamagnetic particles (*8*, *30*). Since the same behavior was observed even at 77 K, in the present work low-temperature measurements were carried out in an attempt to learn more about the structure of the superparamagnetic oxide component.

In Fig. 1 Mössbauer spectra of sample 1 after $CO + H_2$ treatment for 2 days measured at different temperatures are presented. At 79 K (Fig. 1e) the spectrum is characterized by an asymmetric quadrupole doublet with parameters of IS = 0.28 mm s^{-1} and QS = 0.87 mm s^{-1} pointing to the presence of the prevailing iron oxide fraction in the sample. By lowering the temperature of the measurements hyperfine splitting can be observed with an internal field of 443 kOe at 1.9 K. In addition to the sextet, a superparamagnetic line can also be seen at 0.0 mm s^{-1} which is characteristic of a zerovalent iron component. It is of interest that the iron carbide component is

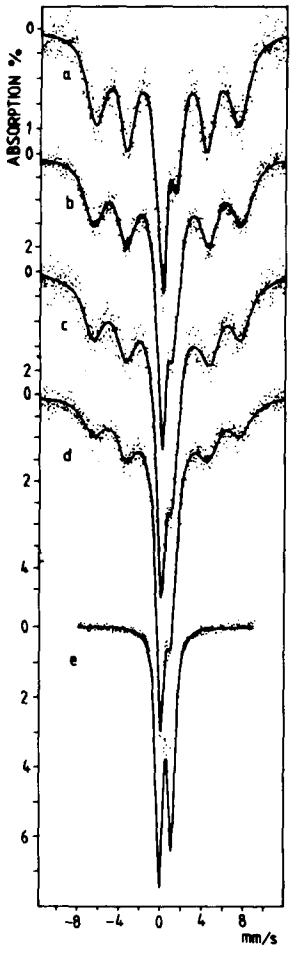

FIG. 1. Mössbauer spectra of sample 1 after CO + H_2 reaction. The spectra are measured at (a) 1.9 K, (b) 4.0 K, (c) 5.4 K, (d) 7.2 K, (e) 79 K.

completely missing from the spectrum in agreement with an earlier finding (*10*).

After high-temperature reduction in hydrogen, a similar structure for the oxide component can be observed in sample 2 (Fig. 2a). In curve b of Fig. 2 the low-temperature spectrum of sample 4 after reduction in hydrogen is also presented. In accordance with other literature data neither a paramagnetic component nor a hyperfine splitting of ferromagnetic iron particles can be seen but the resulting spectrum is indicative of iron oxide particles with an internal magnetic field of 454 kOe, similarly to what was observed in the impregnated state (*8*).

The most relevant parameters of the oxide component are presented in Table 2.

In the presence of ruthenium, and after reduction in hydrogen at 650 K, besides the sextet which is assigned to the iron oxide component, a single line can be observed at IS = 0.0 mm s^{-1}. The spectrum of the reduced iron–ruthenium sample closely resembles that measured after high-temperature reaction in a CO + H_2 mixture (compare Fig. 1 and Fig. 2, curve a).

The following experiments are focused on whether the single component at 0.0 mm s^{-1} can be assigned to highly dispersed monometallic iron particles or whether ru-

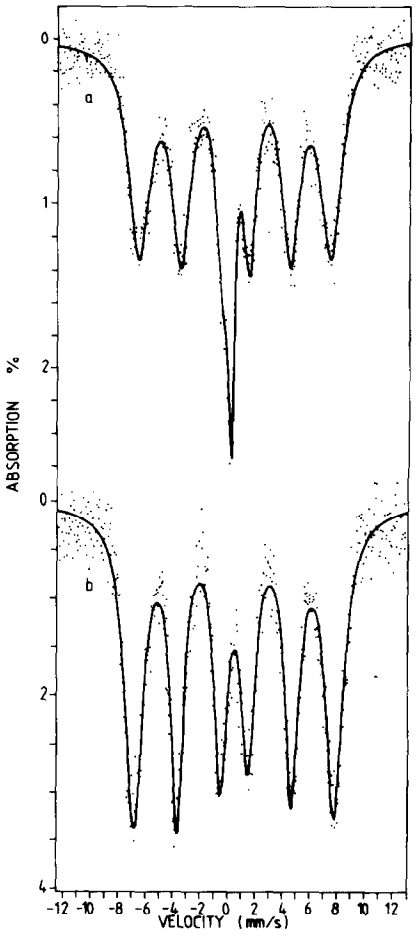

FIG. 2. Mössbauer spectra of (a) sample 2 measured at 4.3 K after reduction in hydrogen at 650 K; (b) sample 4 measured at 1.6 K after reduction in hydrogen.

TABLE 2

The H Magnetic Splitting (kOe), the IS Isomer Shift (mm s^{-1}), and the Relative Intensity (%) of the Total Fe^{3+} Component Measured at 1.8 K after Different Treatments on the Silica-Supported Samples (H_0 = 0)

Treatment		Sample	
		1,2	4
Reduction in H_2	H	431	454
	IS	0.52	0.45
	I_r	98.9	100

thenium atoms are also incorporated in them forming bimetallic particles. One of the fundamental points in the present work is the formation of bimetallic particles after high-temperature reduction. However, it is also important to find out whether the bimetallic particles are maintained or not during the catalytic reaction.

Application of an external magnetic field may help us in solving the problem of bimetallic particles. Thus, if separate superparamagnetic iron particles are present along with separate ruthenium particles, the use of a low magnetic field (~1 T) results in a complete splitting of the single line. If, however, iron particles are associated with ruthenium to form bimetallics, their behavior is no longer expected to be ferromagnetic, in which case relatively large values of H_0 will be necessary to generate resolved hyperfine split spectra. Hence, the influence of external magnetic fields on the shape of the Mössbauer spectra was studied for ruthenium-containing samples 1 and 2. Since the Ru/Fe ratio was the highest for these samples, formation of iron–ruthenium bimetallic particles could be expected. High-field measurements were not carried out on samples 3 and 4. Sample 4 does not contain ruthenium, so the presence of bimetallic particles cannot be expected. Since the Ru/Fe ratio of sample 3 was the lowest (1.6) and the catalytic reaction took place with a 3 : 1 CO : H_2 mixture, a large part of the bimetallic clusters decomposed as is indicated by the carbide species formed.

Mössbauer spectra of sample 2 were recorded in fields of zero and 6 T at 1.5 K (Fig. 3). On fitting the spectra by one sextet, H_{int} = 411 kOe and 419 kOe were obtained at zero and 6 T field, respectively. The full width at the half maximum (FWHM) value of the outermost lines increased by 26% when an external field was applied. The intensity ratio of peaks 2–5 to 1–6 in the sextets decreased from 0.73 to 0.48 under the effect of a 6-T external field. This is the result of polarization of the magnetic moments in the sample to a direction parallel to H_0 (and therefore to the direction of gamma ray propagation). This leads to diminution of the $\Delta m_I = 0$ transitions (lines 2 and 5 in the spectrum) owing to their $\sin^2\theta$ dependence (θ is the angle between the γ-ray propagation and H_0).

In sample 2 the single line at 0.0 mm s^{-1} and with 4.7% relative intensity (H_0 = 0) is split for H_0 = 6 T with a separation of 1.8 mm s^{-1}. The increase of the intensity ratio of the innermost (3–4) lines to the outermost 1–6 lines from 0.40 for H_0 = 0 to 0.47 for H_0 = 6 T indicates that the line recorded

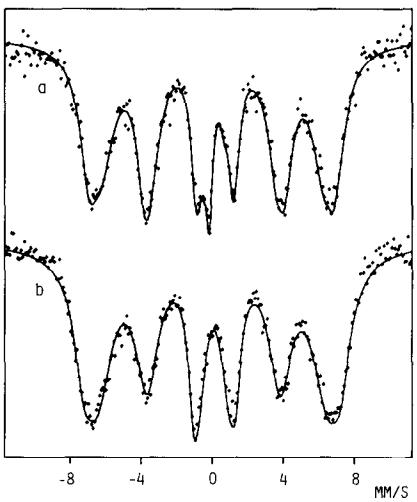

FIG. 3. Mössbauer spectra of sample 2 in external magnetic field at 1.5 K. (a) 0 T, (b) 6 T.

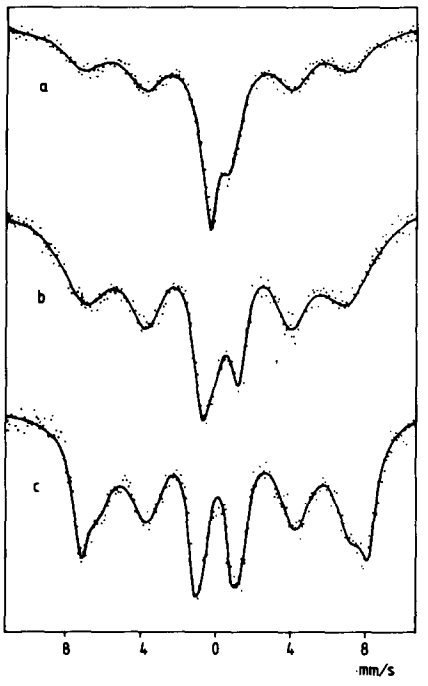

FIG. 4. Mössbauer spectra of sample 1 in external magnetic field at 4.2 K. (a) 0 T, (b) 2 T, (c) 6 T.

at 0.0 mm s^{-1} after splitting is overlapped with the innermost lines of the sextet characteristic of iron oxide.

Since splitting of the central single line was observed in the case of a 6-T field, the Mössbauer spectra of sample 2 were measured for H_0 values of 0, 2, and 6 T field at 4.2 K (Fig. 4). Besides the superparamagnetic and the magnetically split components of iron oxide, a single line at IS = 0.0 mm s^{-1} (about 4%) appeared. Without a magnetic field the FWHM of the single line is 0.51 mm s^{-1}. In a 2-T field its width increases to 1.9 mm s^{-1} (or alternatively the line can be decomposed to a doublet whose separation is 0.52 mm s^{-1}). On a 6-T field its splitting further increases to 2 mm s^{-1} and it is incorporated into the two central lines of the magnetically split sextet and superparamagnetic doublet of iron oxide.

The final state of the samples was also investigated after high-temperature reduction by ferromagnetic resonance. First, a comparison was made of the signal intensities for the different samples. At 123 K we obtained the approximate values of 10^{-2}, 10^{-3}, 10^{-1}, and 1, for samples 1, 2, 3, and 4, respectively, i.e., the intensity manifested itself as being inversely related to the ruthenium content.

The dependence of the relative signal intensity on temperature is shown in Fig. 5. Samples 1 and 2 exhibited a nearly temperature independent behavior while the plots for samples 3 and 4 shown I_r–T curves typical for very small superparamagnetic iron particles. Based on these intensity measurements we can estimate the value of the average size of the metallic iron particles of sample 4.

The temperature dependence of the signal width is seen in Fig. 6. Samples 1 and 2 again show only slight temperature dependence. Curves obtained for samples 3 and 4 reveal the collective behavior of the magnetic moments. For magnetically independent small spherical particles the temperature dependence of ΔH_{pp} is proportional to $K_{1,T}/M_{S,T}$ (*23*), where $K_{1,T}$ is the crystalline anisotrophy energy constant and $M_{S,T}$ is the saturation magnetization at temperature T. On sample 4 the observed signal width values are only 1/5 of the value for bulk iron at 123 K. This drop is due to the small particle size (*31*). At temperatures above 650 K sample 4 shows paramagnetic behavior (ΔH_{pp} increases with temperature). The decrease of the Curie temperature from that

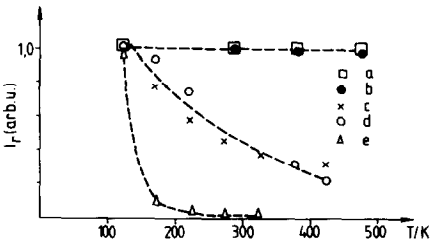

FIG. 5. Temperature dependence of the relative FMR signal intensity after the final reduction. (a) sample 2, (b) sample 1, (c) calculated for 3.0-nm iron particles, (d) sample 4, (e) sample 3.

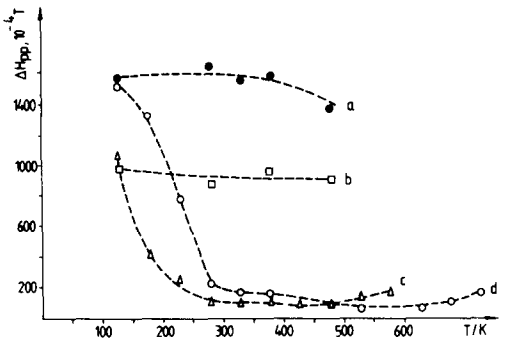

FIG. 6. Temperature dependence of the FMR signal width after the final reduction. (a) sample 1, (b) sample 2, (c) sample 3, (d) sample 4.

of the bulk iron, viz. from 1047 to 650 K, can be regarded as not solely due to the small particle size but also to carbide formation in the CO + H_2 reaction and/or to a low-reduction degree (but no Fe^{3+} signal was found in this sample). ΔH_{pp} for sample 3 decreases more rapidly with temperature than that for sample 4 because the formation of alloys has a greater influence on $K_{1,T}$ than on $M_{S,T}$. On this sample the decrease of the width reversed to increase at about 475 K.

DISCUSSION

It is a surprising but well-proven result that reduction of Fe^{3+} to metallic iron takes place in the presence of noble metals, but even after high-temperature reduction some Fe^{3+} oxide remains in the system. This feature is valid for iron–platinum (*5*, *32*), iron–palladium (*33*), iron–ruthenium (*4*), iron–rhodium (*4*, *34*), and iron–iridium (*35*) samples. It is therefore expected that in the present work the oxide component in the Mössbauer spectra is always present regardless of whether it is measured after reduction or after long-term high-temperature reaction in CO + H_2. In the latter case, however, formation of the oxide component is not surprising because after CO dissociation some oxygen is retained by the metallic component in oxide form (*36*).

Information on the structure of the oxide component can be obtained from the temperature dependence of the Mössbauer spectra. As shown in Fig. 1e, after the CO + H_2 treatment sample 1 does not display a hyperfine split spectrum at 79 K. However, on the spectra recorded between 1.9 and 7.2 K the oxide component reveals superparamagnetic behavior. The value of the hyperfine field determined from the 1.9 K spectrum is low (443 kOe) and significantly smaller than the value determined after Fischer–Tropsch reaction on iron catalyst on which the field distribution was centered around 480 kOe at 4.2 K (*36*). Silica-supported iron and iron–ruthenium catalysts prepared by the incipient wetness method and reduced in hydrogen also showed the presence of the oxide component with 482 kOe internal field at 77 K (*37*). Although those values are already considerably smaller than that obtained for α-Fe_2O_3 at 4.2 K (544 kOe) (*36*), the values measured here are even smaller and are close to those measured for β- and γ-FeOOH (475 and 460 kOe, respectively) (*37*). Furthermore, the occurrence of other pure oxide phases can probably also be excluded. The presence of γ-Fe_2O_3 could additionally be taken into account, but the value of the hyperfine field on the surface shell of γ-Fe_2O_3 particles (with 9 nm diameter) at 4.2 K is reported as being only 1 or 2% less than that for the interior core (*38*). Taking into account this small decrease we conclude that the main constituent of the oxide component is not γ-Fe_2O_3 in our samples.

High-field Mössbauer measurements provide further details on the magnetic properties of the oxide component. Figures 3 and 4 were recorded below the blocking temperature T_B (T_B is the temperature at which the intensity ratio of the superparamagnetic and the magnetically ordered proportion is 1 : 1). These spectra demonstrate that the main constituent of our oxide component is not Fe_3O_4. The two sublattices in Fe_3O_4 should order in small external fields (<1 T) below T_B. The spectrum presented in Fig. 4b obtained in a 2-T external field shows only partial ordering. Once ordered, the

two sublattices of magnetite have different isomer shifts: the outermost peaks on the low-velocity side are separated but they coincide on the positive velocity side of the spectrum. (*39*). Deconvolution of the spectrum obtained using a 6-T field (Fig. 3c) indicates that the two sextets have the same isomer shifts.

On the basis of the above-mentioned experimental results we cannot assign any definite bulk oxide structure to our obtained parameters. As in our case no perfect oxide structure can be assumed, the value of the hyperfine field is not necessarily equal to that measured for crystalline oxides. The highly dispersed state involves an imperfect surface iron oxide structure and the contributions from the exchange, shape and surface anisotropy to the magnetic anisotrophy constant decrease the value of the hyperfine field (*40*). Moreover, our experimental results do not enable us to clearly distinguish whether the oxide component originates from separate oxide particles or whether it is located on a surface layer of the metallic particles.

The distribution of the hyperfine field is also characteristic of the imperfect structure. For example, when fitting the spectrum of sample 1 in Fig. 3a with a single sextet we obtain for FWHM a high value (1.3 mm s^{-1}). Similarly, as is reported in Ref. (*36*), we assumed the presence of the field distribution, and a calculation was performed on the 1.5 K spectra of Fig. 3. The spectra were decomposed to nine sextets, this being the capacity limit of our fitting procedure. All the linewidths were constrained to be equal and the calculation was based upon 95% of the spectral area. The resulting field distributions are shown in Fig. 7. As can be seen, the field distribution is sensitive to the application of the 6-T external field. The appearance of the two distinct maxima in Fig. 7b also indicates the influence of a field-induced orientation effect.

Evidence for Fe–Ru interaction. High external magnetic field Mössbauer studies

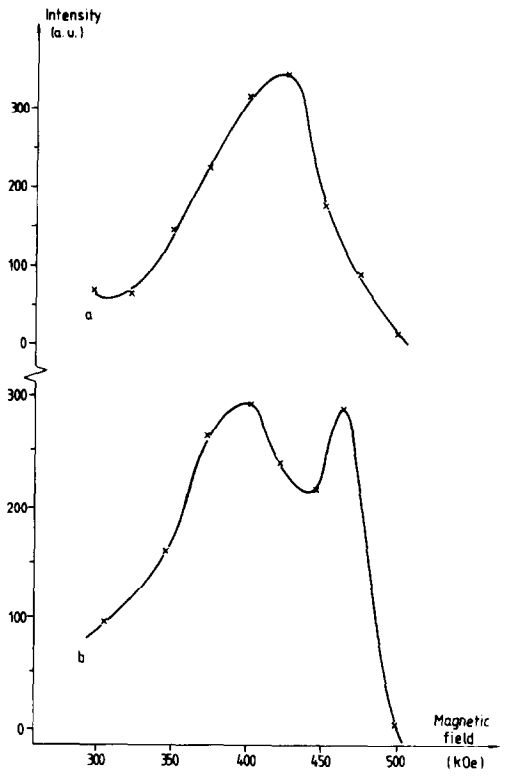

FIG. 7. Magnetic hyperfine field distribution in the particles of sample 2 determined from the spectra of Fig. 3. (a) 0 T, (b) 6 T.

provide evidence for the existence of stable iron–ruthenium bimetallic particles. Figure 1 indicates that part of iron is in the $Fe^{(0)}$ state. This corresponds to the IS = 0.0 mm s^{-1} singlet line in the spectrum recorded after the CO + H_2 reaction on sample 1 (Fig. 1), and after the high-temperature hydrogen reaction of sample 2 (Fig. 2a). This IS ~ 0.0 mm s^{-1} line can be attributed either to superparamagnetic metallic iron particles of high dispersion or to bimetallic iron–ruthenium particles because the isomer shift values of iron–ruthenium alloys are close to 0.0 mm s^{-1} (*41–43*). The structure and the magnetic properties of iron and iron–ruthenium alloys are different. Metallic α-iron is a ferromagnet with bcc crystal structure whereas iron–ruthenium alloys in the 23–100 at.% Ru range have an hcp structure and are Pauli paramagnets above 13 at.%

ruthenium content (*41*). A small splitting in their Mössbauer spectra with the corresponding internal field of 13 kOe has been considered as an indication of weak antiferromagnetic coupling at low temperatures (*42*).

If the line at IS = 0.0 mm s^{-1} were superparamagnetic iron, the spin flipping would be stopped on applying a relatively small magnetic field, and superparamagnetic iron particle would show a hyperfine splitting approaching that of bulk metallic iron (330 kOe). On the contrary, paramagnets exhibit line separation which is proportional to the external field. On samples 1 and 2 the latter phenomenon was observed; the IS ~ 0.0 mm s^{-1} singlet showed a splitting proportional to the applied field. The value of the external fields used considerably exceeded the value of the assumed antiferromagnetic ordering field in the iron–ruthenium particles, thereby enabling them to exhibit paramagnetic behavior. Thus, we conclude the existence of iron–ruthenium bimetallic particles in samples with Ru/Fe ratios of 4 and 6.5.

A further comment should be added to the interpretation of the iron–ruthenium interaction derived from the low-temperature spectra. The IS ~ 0.0 mm s^{-1} component has a relative intensity of only 10% in these low-temperature spectra. Under reaction conditions the relative intensity of this zerovalent component is much higher because the high-temperature reduction of iron ions is enhanced by the ruthenium. In addition, the temperature dependence of the Mössbauer effect is different for the metallic iron and for the supported iron oxide of high dispersion; the recoil-free fraction increases more rapidly for iron oxide than for iron with decreasing temperature (*36*). This is also seen when comparing the spectra of sample 2 recorded at 1.5 and 4.3 K (Figs. 3a and 2a). Thus the low relative percentage of zerovalent iron detected at low temperatures represents a more significant quantity of $Fe^{(0)}$ under the reaction conditions.

The FMR measurements performed on the reduced catalysts provide further proof of the existence of iron–ruthenium bimetallic particles in samples 1 and 2 and they also provide information on the metallic particles of samples 3 and 4. In the FMR spectra only the signals of metallic particles were detected, i.e., no Fe^{3+} signal was found and the presence of Fe_3O_4 can also be excluded for two reasons: (i) no reverse of the sign of $K_{1,T}$ was observed on the recorded signals as would be expected to occur between 123 and 173 K for magnetite (*44*); (ii) the recorded ΔH_{pp} values at low-temperature measurements far exceed the reported signal width values of magnetite (*45*).

Comparison of the signal intensity of the four samples (10^{-2}, 10^{-3}, 10^{-1}, and 1 on samples 1, 2, 3, and 4, resp.) clearly points to the decrease of collective magnetism with increasing ruthenium content, indicating bimetallic particle formation. The slight temperature dependence of I_r and ΔH_{pp} values of samples 1 and 2 is in full accordance with the Pauli paramagnetic behavior of the Fe–Ru bimetallic particles mentioned previously.

The small particles of lower ruthenium content of sample 3 and iron particles of sample 4 exhibited superparamagnetic temperature dependence corresponding to the Langevin or Curie function (*24*). A simple calculation can be performed on the data obtained on sample 4 to determine the average particles size. If we apply the Langevin function, $L(x)$ (where $x = MvH_{eff}/kT$, M the magnetization and v the particle volume), to describe the temperature dependence of the signal intensity, the intensity values obtained at temperature T and $T/2$ may be compared. In this case the following relation holds (46): $L(2x)/L(x) = I_r^{T/2}/I_r^T = a$. On extracting the values of a from the experimental values of x, the average particle volume can be calculated. A value of 3.0 nm was found in this way for the average diameter of the iron particles of sample 4. The crosses in Fig. 5 represent the calculated relative intensity values of 3.0-nm iron par-

ticles at different temperatures. The coincidence with the measured curve for sample 4 is acceptable.

CONCLUSIONS

On silica-supported iron and iron–ruthenium catalysts oxide and metallic components were found from Mössbauer measurements performed after CO + H_2 reaction and hydrogen reduction on samples with Ru/Fe ratios of 3.9 and 6.5. As indicated by the low-temperature spectra the oxide component cannot be assigned to perfect crystalline structure.

Clear evidence is obtained for the existence of paramagnetic iron–ruthenium bimetallic particles from Mössbauer and FMR studies performed on the mentioned samples. The experimental verification of bimetallic particles is in full agreement with the results derived from previous catalytic activity and selectivity measurements.

FMR studies carried out on reduced samples of low Ru/Fe ratios also revealed the presence of ferromagnetic particles and 3.0 nm is estimated for the average value of the particle diameter for the supported iron sample.

ACKNOWLEDGMENTS

The authors are grateful to A. Vizi-Orosz for the preparation of the ^{57}Fe carbonyl clusters and to M. Szökefalvi-Nagy for the XRF measurements. This work was supported in part by the NSF Solid State Chemistry program, Grants DMR 8016441 and DMR 8313710.

REFERENCES

1. Good, M. L., Patil, M. D., Donner, J. T., and Madhusudahan, C. P., *Adv. Chem.* **194,** 553 (1981).
2. Ott, G. L., Fleisch, T., and Delgass, W. N., *J. Catal.* **60,** 394 (1979).
3. Vannice, M. A., Lam, Y. L., and Garten, R. L., *Adv. Chem.* **178,** 25 (1979).
4. Niemantsverdriet, J. W., Aschenbeck, D. P., Fortunato, F. A., and Delgass, W. N., *J. Mol. Catal.* **25,** 285 (1984).
5. Dézsi, I., Nagy, D. L., Eszterle, M., and Guczi, L., *J. Phys. (Paris)* **40,** C2-76 (1979).
6. Good, M. L., Akbarnejad, M., and Donner, J. T., *Prepr., Amer. Chem. Soc., Div. Pet. Chem.* **25,** 763 (1980).
7. Guczi, L., Schay, Z., Matusek, K., Bogyay, I., and Stefler, G., *in* "Proceedings, 7th International Congress on Catalysis, Tokyo, 1980," p. 211. Elsevier, Amsterdam/Kodansha, Tokyo (1981).
8. Lázár, K., Matusek, K., Mink, J., Dobos, S., Guczi, L., Vizi-Orosz, A., Markó, L., and Reiff, W. M., *J. Catal.* **87,** 163 (1984).
9. Schay, Z., Lázár, K., Mink, J., and Guczi, L., *J. Catal.* **87,** 179 (1984).
10. Lázár, K., Schay, Z., and Guczi, L., *J. Mol. Catal.* **17,** 205 (1982).
11. Schay, Z., and Guczi, L., *Acta Chim. Acad. Sci. Hung.* **111,** 607 (1982).
12. Guczi, L., Schay, Z., and Lázár, K., *Surf. Sci.* **106,** 516 (1981).
13. Böszörményi, I., Dobos, S., Guczi, L., Markó, L., Lázár, K., Schay, Z., Takács, L., Vizi-Orosz, A., and Reiff, W. M., *in* "Proceedings, 8th International Congress on Catalysis, Berlin, 1984," Vol. V, p. 183. Verlag Chemie, Weinham, 1984.
14. Choplin, A., Leconte, M., Basset, J. M., Shore, S. G., and Hsu, W. I., *J. Mol. Catal.* **21,** 389 (1983).
15. Budge, R., Lücke, B. F., Scott, J. P., and Gates, B. C., *in* "Proceedings, 8th International Congress on Catalysis, Berlin, 1984," Vol. V, p. 89. Verlag Chemie, Weinheim, 1984.
16. Kaminsky, M., Yoon, K. J., Geoffroy, G. L., and Vannice, M. A., *J. Catal.* **91,** 338 (1985).
17. Blanchard, F., Reymond, J. P., Pommier, B., and Teichner, S. J., *J. Mol. Catal.* **17,** 171 (1982).
18. Christensen, P. H., Mørup, S., Clausen, B. S., and Topsøe, H., *in* "Proceedings, 8th International Congress on Catalysis, Berlin, 1984," Vol. II, p. 545. Verlag Chemie, Weinheim, 1984.
19. Jung, H-J., Vannice, M. A., Mulay, L. N., Stanfield, R. M., and Delgass, W. N., *J. Catal.* **76,** 208 (1982).
20. Morrish, A. H., Physical Principles of Magnetism, p. 539. Wiley, New York, 1965.
21. Tsay, F. D., Chan, S. I., and Manatt, S. I., *Geochim. Cosmochim. Acta* **35,** 865 (1971).
22. Engels, S., and Mörke, W., *Phys. Status. Solidi B* **119,** K109 (1983).
23. Griscom, D. L., *J. Non-Cryst. Solids* **67,** 81 (1984).
24. Romanowski, W., *Z. Anorg. Allg. Chem.* **351,** 180 (1967).
25. Robertson, S. D., Kloet, S. C., and Sachtler, W. M. H., *J. Catal.* **39,** 234 (1975).
26. Hugues, F., Dalmon, J. A., Bussière, P., Smith, A. K., Basset, J. M., and Olivier, D., *J. Phys. Chem.* **86,** 5136 (1982).
27. Rojas, D., Bussière, P., Dalmon, J. A., Choplin, A., Basset, J. M., and Olivier, D., *Surf. Sci.* **156,** 516 (1985).
28. Kulcsár, K., Nagy, D. L., and Pócs, L., Central Research Institute for Physics Report 1971-67. Budapest, Hungary.

29. Guczi, L., Böszörmènyi, I., Dobos, S., Lázár, K., Takács, L., and Schay, Z., *in* "Reactivity of Solids" (P. Barret and L. C. Dufour, Eds.), p. 1087. Elsevier, Amsterdam, 1985.
30. Guczi, L., *J. Mol. Catal.* **25,** 13 (1984).
31. de Biasi, R. S., and Devezas, T. C., *Phys. Lett. A* **50,** 137 (1974).
32. Vannice, M. A., and Garten, R. L., *J. Mol. Catal.* **1,** 201 (1975/76).
33. Garten, R. L., and Ollis, D. F., *J. Catal.* **35,** 232 (1974).
34. Niemantsverdriet, J. W., van der Kraan, A. M., and Delgass, W. N., *J. Catal.* **89,** 138 (1984).
35. Murrel, L. L., and Garten, R. L., *Appl. Surf. Sci.* **19,** 218 (1984).
36. Niemantsverdriet, J. W., Flipse, C. F. J., van der Kraan, A. M., and van Loef, J. J., *Appl. Surf. Sci.* **10,** 302 (1982).
37. Eszterle, M., and Guczi, L., *Magy. Kém. Lapja,* **36,** 429 (9181).
38. Haneda, K., and Morrish, A. H., *Phys. Lett. A* **64,** 259 (1977).
39. Mørup, S., Dumesic, J. A., and Topsøe, H., *in* "Applications of Mössbauer Spectroscopy" (R. Cohen, Ed.), Vol. 2. Academic Press, New York, 1980.
40. Mørup, S., *J. Magn. Magn. Mater.* **37,** 39 (1983).
41. Fujimori, H., and Saito, H., *J. Phys. Soc. Japan* **26,** 1115 (1969).
42. Williams, J. M., and Pearson, D. I. C., *J. Phys. (Paris)* **37,** C6-401 (1976).
43. Rush, J. D., Johnson, C. E., and Thomas, M. F., *J. Phys. F* **6,** 2017 (1976).
44. Bickford, L. R., *Phys. Rev.* **78,** 449 (1950).
45. Kneller, E., "Ferromagnetismus," p. 151. Springer, Berlin, 1962.
46. Mörke, W., and Drews, H., *Z. Chem.*, in press.